

Automated Arteriole and Venule Recognition in Retinal Images using Ensemble Classification

M. M. Fraz¹, A. R. Rudnicka², C. G. Owen², D. P. Strachan² and S. A. Barman¹

¹*School of Computing and Information Systems, Faculty of Science Engineering and Computing, Kingston University London, London, U.K*

²*Division of Population Health Sciences and Education, St. George's, University of London, London, U.K*

Keywords: Medical Image Analysis, Retinal Image Processing, Artery Vein Classification, Ensemble Learning.

Abstract: The shape and size of retinal vessels have been prospectively associated with cardiovascular outcomes in adult life, and with cardiovascular precursors in early life, suggesting life course patterning of vascular development. However, the shape and size of arterioles and venules may show similar or opposing associations with disease precursors / outcomes. Hence accurate detection of vessel type is important when considering cardio-metabolic influences on vascular health. This paper presents an automated method of identifying arterioles and venules, based on colour features using the ensemble classifier of boot strapped decision trees. The classifier utilizes pixel based features, vessel profile based features and vessel segment based features from both RGB and HIS colour spaces. To the best of our knowledge, the decision trees based ensemble classifier has been used for the first time for arteriole/venule classification. The classification is performed across the entire image, including the optic disc. The methodology is evaluated on 3149 vessel segments from 40 colour fundus images acquired from an adult population based study in the UK (EPIC Norfolk), resulting in 83% detection rate. This methodology can be further developed into an automated system for measurement of arterio-venous ratio and quantification of arterio-venous nicking in retinal images, which may be of use in identifying those at high risk of cardiovascular events, in need of early intervention.

1 INTRODUCTION

With the development of digital imaging and computational efficiency, image processing, analysis and modeling techniques are increasingly used in all fields of medical sciences, particularly in ophthalmology (Abramoff, Garvin et al. 2010). Automated detection of micro-vascular disease such as diabetic retinopathy in the retinal image using digital image analysis methods has huge potential benefits in screening programs for early detection of disease (Fraz, Remagnino et al. 2012). The blood vessel structure in retinal images is unique in the sense that it is the only part of the blood circulation system that can be directly observed non-invasively, can be easily imaged using Fundus cameras. Morphological characteristics of retinal blood vessels (particularly width) have been prospectively associated with cardiovascular outcomes in adult life (Wong, Klein et al. 2001), and with cardio-metabolic risk factors in early life (Owen, Rudnicka

et al. 2011). Associations between retinal vessel morphology and disease precursors / outcomes may be similar or opposing for arterioles and venules. For instance, hypertension and atherosclerosis may have different effects in retinal arterioles and venules, resulting in a decreased arteriole to venule width ratio (AVR) (Jack J. Kanski and Brad Bowling 2011). Retinal arteriovenous nicking, a pathognomonic sign of hypertension, is another retinal feature worthy of study, characterized by a decrease in the venular calibre at both sides of an artery-vein crossing (Jack J. Kanski and Brad Bowling 2011). However, more subtle changes in arteriole / venular morphology may be an early physio-maker of vascular health, which might predict those at high risk of disease in middle and later life. However, identifying small changes in retinal arterioles and venules is a difficult task to perform manually, as it is subjective, open to measurement error, and time consuming, limiting its use in large population based studies. Automated

segregation of retinal arterioles and venules could be used to assist with this task, which would be a pre-requisite for the development of a computer assisted tool for use in large populations to identify those at high risk of disease.

The appearance of arterioles and venules in retinal images are similar. The general assumption is that there is a difference in the colour and size of the venules and arterioles; the later one appears to be thinner, brighter and present more frequently with a central light reflex. However, there are some challenges in building a robust vessel classification system. There is intra-image and intra-subject variance in the blood colour. The size and colour of similar blood vessels changes as they move away from the optic disc. In the periphery vessels become so this they are almost indistinguishable. The context based features may also fail at these locations due to vessel crossings and branching. In addition, the curved shape of the retina and non-uniform illumination add complexity to the automated vessel classification task.

A number of methods have been reported in literature for retinal arteriole/venule (a/v) classification, which can be divided into two broad categories; automated and semi-automated methods. In automated methods (Niemeijer, Xiayu et al. 2011; Huang, Zhang et al. 2012; Dashtbozorg, Mendonca et al. 2013; Nguyen, Bhuiyan et al. 2013), the vessel centerline pixels forming the vascular skeleton are extracted from the segmented vascular tree, followed by the calculation of various distinguishable features for each centerline pixel and finally each pixel is assigned as an arteriole or venule by a classifier. In semi-automated methods (Rothaus, Jiang et al. 2009; Vázquez, Cancela et al. 2013), the initial pixels on the main vessels are marked as arteriole or venule by an expert, and then these labels are propagated across the vascular network through vessel tracking using the structural characteristics and connectivity information.

Grisan's method (Grisan and Ruggeri 2003) was amongst the first to propose automatic a/v separation. The main idea was to divide the optic disc centered images into four quadrants with the assumption that each quadrant will contain approximately the same number of arterioles and venules with significant differences in the features. The variance of the red channel and mean of the hue are used as vessel features, fuzzy clustering is applied to each partition independently. In another method (Saez, González-Vázquez et al. 2012), the quadrants are rotated in steps of 20 degrees with the aim of fulfilling the assumption that each quadrant

should contain at least one venule and one arteriole. K-Means clustering is used to classify the vessels in two concentric circumferences around the optic disc. The quadrant-wise classification enforces a condition to have at least one arteriole and one venule per quadrant and it seems more suitable for optic disc centered images rather than macula centered images. Also, basic K-Means clustering is sensitive to the initialization and may often become stuck at a local optimal.

In this paper we have presented an automated method for retinal a/v classification utilizing an ensemble classifier of boot strapped decision trees. The classifier based on the boot strapped decision trees is a classic ensemble classifier, which has been broadly applied in many application areas of image analysis (Fraz, Remagnino et al. 2012), but has not been extensively utilized for retinal vessel classification. To our knowledge, this is the first use of a decision trees based ensemble method for a/v classification. An important feature of the bagged ensemble is that the classification accuracy can be estimated during the training phase, without supplying the classifier with test data. Moreover, the importance of each feature in classification can also be predicted during the training phase, which helps in identifying the most relevant features used in a/v classification thus automatically reducing the dimensionality of the feature vector and boosting computational speed. The method is validated on 40 macula centered fundus photographs acquired from 20 middle-aged and elderly adults examined as part of the latest phase of the European Investigation into Cancer in Norfolk study (EPIC-Norfolk 2013). The classification is not only performed near the optic disc but across the entire image. The proposed method achieves a high classification rate without increasing the training samples or adding many features.

The organization of the paper is as follows. Section 2, presents the methodology for automated segmentation of retinal blood vessels. Next, the vessel classification methodology is explained in section 3. Section 4 presents the validation methodology and experimental results. Finally, the discussion and conclusions are given in Section 5.

2 THE METHODOLOGY

The vascular network is segmented from the coloured retinal image and the vascular skeleton consisting of centerline pixels is constructed. Vessel segments are generated by search and removal of

bifurcations crossing points. For each centerline pixel in the vessel segment, the feature vector is computed using pixel based features, profile based features and vessel segment based features of the RGB and HSI colour spaces, and finally each centerline pixel is assigned an artery or vein label by a decision tree based ensemble classifier.

2.1 Retinal Vessel Segmentation

The retinal vasculature is composed of arterioles and venules, appearing as piecewise linear features, with variation in width and their branches visible within the retinal image (Fraz, Barman et al. 2012). We have computed a measure of vessel-ness for each pixel in the retinal image by combining a multi-scale line detection which is calculated from the inverted green plane of the coloured retinal images. The average pixel intensity is measured along lines of a particular length passing through the pixel under consideration at 12 different orientations spaced by 15 degrees each. The line with the highest average pixel intensity is selected. The line strength of a pixel is calculated by computing the difference in the average grey values of a square sub-window centred at the target pixel with the average intensity of the selected line. This concept was first introduced by (Ricci and Perfetti 2007) and has also been employed elsewhere (Fraz, Remagnino et al. 2012). We have used a generalized multi-scale line detector (Nguyen, Bhuiyan et al. 2012), which uses a variable length of aligned lines in a fixed square sub-window, for calculating the line strength measures for the pixels in the images containing a central vessel reflex. In the line strength image (LSI), each value corresponds to the confidence measure of each pixel to be a part of the vessel or not. The LSI, as illustrated in Figure 1(b), is often considered as a greyscale image, where bright pixels indicate a higher probability of being a vessel pixel.

In order to obtain a vessel binary segmentation, a hysteresis thresholding based morphological reconstruction is applied. Hysteresis thresholding employs a bi-threshold procedure such that the intensity image is thresholded for two ranges of grey values, one being included in the other. The image is first segmented by a narrow threshold range which concedes only high confidence object pixels and thus also contains many false negatives. This image is termed a *marker image*. The *mask image* is generated by applying a wide threshold range to the greyscale image. These threshold values are derived from the intensity histogram of the non-null pixels; each one of these thresholds; T_1 for the *marker*

image and T_2 for the *mask image*, is defined as the highest intensity value such that the number of pixels with intensities above this limit is greater or equal to a predefined percentage. This percentage value is empirically selected for T_1 and T_2 as 90% and 95% respectively.

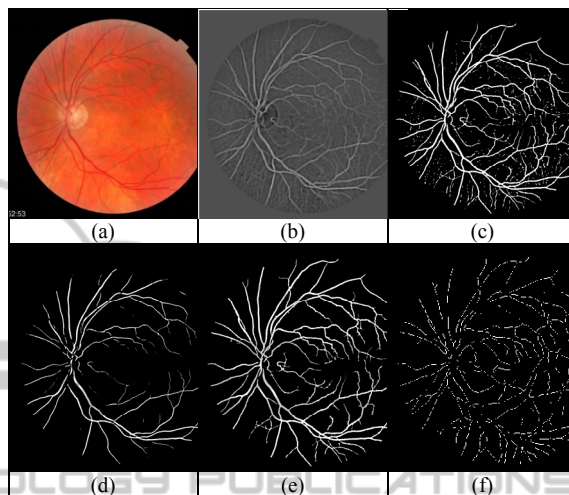


Figure 1: (a) Coloured retinal image, (b) Line strength image, (c) Marker Image, (d) Mask Image, (e) Segmented vascular, (f) Extracted Vessel segments.

The image is first segmented by a narrow threshold range which concedes only high confidence object pixels and thus also contains many false negatives. This image is termed a *marker image*. The *mask image* is generated by applying a wide threshold range to the greyscale image. These threshold values are derived from the intensity histogram of the non-null pixels; each one of these thresholds; T_1 for the *marker image* and T_2 for the *mask image*, is defined as the highest intensity value such that the number of pixels with intensities above this limit is greater or equal to a predefined percentage. This percentage value is empirically selected for T_1 and T_2 as 90% and 95% respectively. The *marker* image is used as a seed for the morphological reconstruction using the *mask image*. Figure 1(c-e) shows the marker, mask and segmented vessels image respectively.

2.2 Vessel Segment Extraction

The skeletonization is applied to the binary segmented vasculature image which reduces all the vessels to a single centreline one pixel wide. The bifurcation points and crossing points are detected in the vessel centreline image by counting the neighbourhood of each pixel. The vessel centreline

image is scanned to analyse the neighbours of each pixel for eight-connectivity. This way, the intersection number, $In(x, y)$ is calculated for each pixel $p(x, y)$ of the centreline image, as shown in equation (2).

$$In(x, y) = 0.5 * \left[\sum_i^8 |N_i(x, y) - N_{i+1}(x, y)| \right] \quad (1)$$

where $N_i(x, y)$ are the neighbours of the analysed point, $p(x, y)$.

According to its intersection number In each pixel $p(x, y)$ will be marked as vessel end point if $In(x, y)=1$, vessel internal point if $In(x, y)=2$, bifurcation if $In(x, y)=3$ and crossover if $In(x, y)=4$.

The detected bifurcation points and crossing points are deleted from the vessel centreline image and the retinal vasculature is cut into the vessel segments as shown in Figure 1(f).

2.3 Image Normalization and Shade Correction

The absolute colour of the blood in the vessels varies between the images and across the subjects. To overcome this variability some authors (Grisan and Ruggeri 2003; Saez, González-Vázquez et al. 2012) have used a quadrant based approach which is computationally intense, also it enforces a condition to have at least one arteriole and one venule per quadrant, and it seems more suitable for optic disc centered images rather than macula centered images.

We have used a simple linear transformation for shade correction and variability normalization. For this purpose, the estimate of the background o is obtained by applying a filtering operation with a large arithmetic mean kernel. The size of the filter kernel is not a critical parameter as long as it is large enough to ensure the blurred image contains no visible structures such as vessels. In this work, we use a 121×121 pixel size kernel. Then the difference between the morphologically opened image I_o and the estimated background I_{BE} is then computed for each pixel to obtain a normalized image I_n .

$$I_n(x, y) = I_o(x, y) - I_{BE}(x, y) \quad (2)$$

Likewise, when the fluctuation in background intensity of retinal images is examined, there can be significant variation in intensities between images due to different illumination conditions in the acquisition process. Therefore, a shade corrected image is obtained by applying a global transformation with the purpose of reducing the

intensity variation and contrast enhancement. For this purpose, the pixel intensities are modified according to the following global linear transformation function,

$$I_H(x, y) = \begin{cases} 0, & \text{if } I_n(x, y) < 0 \\ 1, & \text{if } I_n(x, y) > 1 \\ p(x, y), & \text{otherwise} \end{cases} \quad (3)$$

$$p(x, y) = I_n(x, y) + 0.5 - val_{MAX_PIXEL}$$

where, $I_H(x, y)$ is the homogenized image, $I_n(x, y)$ is the normalized image shown in (7), val_{MAX_PIXEL} is the intensity value presenting the highest number of pixels in the normalized image $I_n(x, y)$. The pixels with intensity value equal to val_{MAX_PIXEL} belong to the background of the retinal image. This global transformation will set them to 0.5 and will standardize the intensity around this value of those background pixels with different illumination conditions. In order to find differences between arterioles and venules, we have analysed RGB and HIS colour spaces. Figure 2 shows the red, green and blue components of the image shown in Figure 1(a) along with respective shade corrected images.

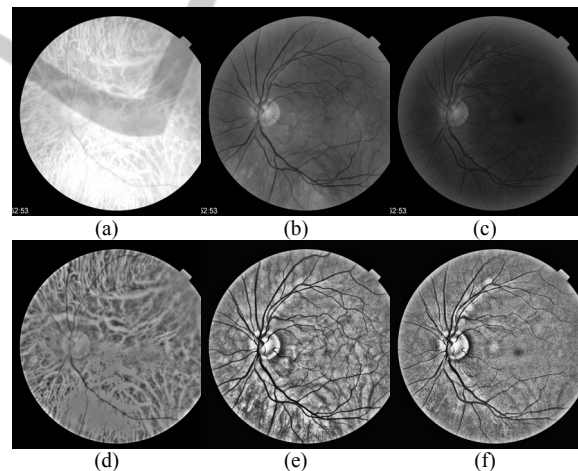


Figure 2: The colour spaces; (a-c) Red, Green and Blue channels of RGB. (d-f) the shade corrected images of Red green and blue channels respectively.

2.4 Feature Extraction

In previous work (Fraz, Remagnino et al. 2013), we have computed the local orientation angle of vessel segment and the width of vessel for each centreline pixel. Based on this information we have extracted the vessel profile for each centreline pixel. The vessel profile is perpendicular to vessel direction, and the length of vessel profile is equal to the vessel width. The centreline, edges and the vessel segment

profiles are shown in Figure 3(a). We define three types of features extracted from the vessel segments for each centreline pixel: pixel based features, profile based features and vessel segment based features.

The pixel based features are the centreline pixel intensity values taken from the respective colour channel. The profile based features are the mean and variance of the intensity values across a vessel profile for each centreline pixel. The vessel segment based features are calculated in two ways for each centreline pixel from the respective colour channel. First, the mean and variance of the pixel intensities are calculated for the entire vessel segment. Second, the relatively longer vessel segments are divided into smaller vessel parts of length of almost 50 pixels, and then the mean and variance of the pixel intensities are calculated with in these vessel . We have tried and tested the different size of vessel sub-segments ranging from 15 to 75 pixels and achieve the best results using 50 pixels.

Figure 3(b) illustrates a vessel segment where the edges are marked with blue lines and the centreline pixels (C_i) are shown with green circles on the black line. The vessel profile (P_i) consists of the pixels in the line drawn perpendicular to the local vessel direction, equal to the approximate vessel width, and is shown in white. VP_i are the vessel segment parts. Table 1 shows the complete set of features extracted for each centreline pixel.

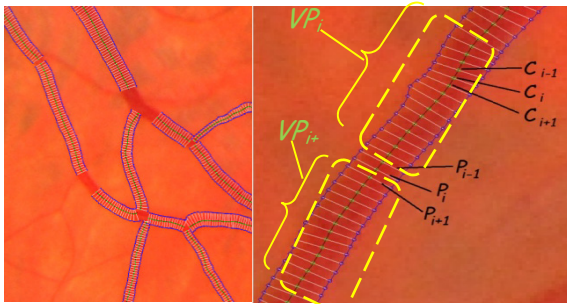


Figure 3: (a) Vessel profiles; (b) Vessel Features for A/V classification.

The feature set (f_v) can be summarized as follows.

$$\begin{aligned}
 f_v(n) &= X[C_i] \quad \forall C_i \in \text{vessel segment} \\
 f_v(n) &= \mu(X[P_i]) \quad \forall P_i \in \text{vessel segment} \\
 f_v(n) &= \sigma(X[P_i]) \quad \forall P_i \in \text{vessel segment} \\
 f_v(n) &= \mu(X[VP_i(x,y)]) \quad \forall VP_i \in \text{vessel segment} \\
 f_v(n) &= \sigma(X[VP_i(x,y)]) \quad \forall VP_i \in \text{vessel segment} \\
 f_v(n) &= \mu(X[I(x,y)]) \quad \forall \text{pixels}(x,y) \text{ in vessel segment} \\
 f_v(n) &= \sigma(X[I(x,y)]) \quad \forall \text{pixels}(x,y) \text{ in vessel segment}
 \end{aligned}$$

Table 1: Complete set of features extracted for each centreline pixel.

No.	Feature description	Type
1-6	The centreline pixel intensity values from each component of RGB and HSI colour space	Pixel based
7-12	Mean of pixel intensities of vessel part VP_i from each colour component of RGB and HSI.	Vessel segment part based features
13-18	Standard deviation of pixel intensities of vessel part VP_i from each colour component of RGB and HSI.	
19-22	Min and Max values of pixel intensities of vessel segment part VP_i from each R and G component	
23-25	Mean of pixel intensities of vessel profiles P_i from each colour component of RGB	Vessel profile based features
26-31	Standard deviation of pixel intensities of vessel profiles P_i from each colour component of RGB and HSI.	
32-35	Min and Max values of pixel intensities of vessel profiles P_i from R and G component.	
36-41	Mean of pixel intensities of complete vessel segment from each component of RGB and HSI.	Vessel segment based features
42-47	Standard deviation of pixel intensities of complete vessel segment from each colour component of RGB and HSI.	
48-51	Min and Max values of pixel intensities of complete vessel segment from each R and G component from RGB.	

where, n is the number of features, $X[C_i]$ is the value of the colour channel X at point C_i in the image, $X \in \{R,G,B,H,S,I\}$. For instance, $R[C_i]$ is the value of the centreline pixels in the R colour component, $\mu(G[P_i])$ is the mean of the vessel profile pixels in the green channel.

Figure 4(a) shows the graphs for feature importance index calculated from classifiers created with 30 decision trees and trained with 15000 training samples. Based on the information shown in the graph, five sets of features have been created by selecting those features, where the importance index is more than the following values $\{0.75, 1.0, 1.5, 2.0, 2.75\}$. Five classifiers have been trained with the reduced feature sets and the out-of-bag (OOB) classification error is computed for each of the classifiers and is plotted in Figure 4(b). It has been observed that the performance of the classifier trained with 16 most significant features is best among all; therefore 16-D is utilized for vessel classification.

2.5 Vessel Labelling

The final labelling of vessel pixels is obtained by employing supervised classification with an ensemble classifier of bagged decision trees. We assume that all the pixels in the vessel segment are either in an arteriole or venule. The classification of

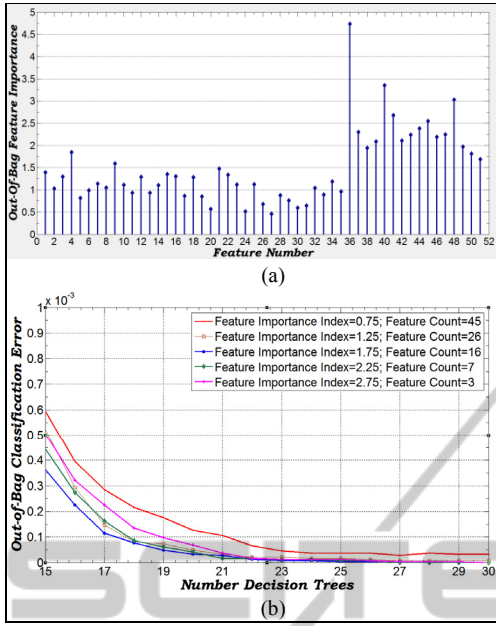


Figure 4: (a) Feature Importance Index, (b) Out-of-Bag classification error with reduced feature sets.

the retinal vessel is a two class classification problem where each pixel in the image either belongs to an artery (C_A) or to a vein (C_V).

In Ensemble classification (Polikar 2006), multiple classifiers or models are tactically generated and combined in order to give the solution to a machine learning problem; with the goal of obtaining better predictive performance than could be obtained from any of the constituent classifiers / models. This process is used to abbreviate the likelihood of inadequate or unfortunate selection while improving the classification or prediction performance of the classifier. We use this strategy instinctively in our day to day activities, where we consider the opinion from several experts, evaluate and merge their recommendations for establishing a well optimized and well-versed conclusion. In the same manner, the ensemble methods utilize multiple classifiers/models to accomplish gain in classification performance by mixing/aggregating the outcomes from several weak learners into one high-class classifier, with the goal of reducing the variance and amplifying the confidence in the decision. In the present work, the decision trees have been used as the component classifier of the ensemble system and which is created by employing boot strapped aggregation

Let us consider a set of observations “ x_n ” from the feature vector with a known class label “ y ” as a training set, where $y \in \{C_A, C_V\}$. The objective is to predict the class label “ y ” for the given observations.

The classifier assigns soft labels to the centreline pixel labels, which can be regarded as a vote for the label of the complete vessel segment, and the mean of these votes is assigned as the label for the entire vessel segment.

3 RESULTS

3.1 Evaluation Criteria and Performance Measures

We have tested this methodology on retinal images obtained from EPIC Norfolk study (EPIC-Norfolk 2013). The dataset contains 40 macula centered retinal images from both of the eyes of 20 study participants, with the vessel types manually labelled by trained observers. The images were captured with non-mydratic fundus cameras and saved in 24-bit JPEG format with a resolution of 3000x2000 pixels. The performance measure are obtained for the centreline pixels in the entire image and evaluated separately for arterioles and venules. For each of the vessel type, the True Positives (TP), False Positives (FP), True Negatives (TN) and False Negatives (FN) are calculated in the same way as in (Saez, González-Vázquez et al. 2012), and tabulated in Table 2.

Table 2: Vessel classification ($Class \in \{a, v\}$).

	Observer Identify pixel $\in Class$	Observer identify pixel $\notin Class$
System Identify pixel $\in Class$	True Positive (TP_{Class})	False Positive (FP_{Class})
System Identify pixel $\notin Class$	False Negative (FN_{Class})	True Negative (TN_{Class})

The algorithm is evaluated in terms of Detection Rate / Sensitivity ($SN_{a|v}$), Specificity ($SP_{a|v}$), Classification Accuracy ($ACC_{a|v}$), Classification Error Rate ($CER_{a|v}$), Positive Predictive Value ($PPV_{a|v}$), Negative Predictive Value ($NPV_{a|v}$) and the Positive and Negative Likelihood Ratios ($PLR_{a|v}$ and $NLR_{a|v}$). The $ACC_{a|v}$ is measured by the ratio of the total number of correctly classified pixels (sum of true positives and true negatives) by the number of pixels under consideration in the image. $SN_{a|v}$ reflects the ability of an algorithm to detect the true positives. $SP_{a|v}$ measures the proportion of negatives that are correctly identified. $PPV_{a|v}$ or precession rate gives the proportion of vessel pixels with correctly identified positive test results and $NPV_{a|v}$ is the proportion of vessel pixels with negative test results

that are correctly identified. The predictive values depends on the percentage of a/v in the retina (prevalence), therefore the likelihood ratios ($PLR_{a/v}$ and $NLR_{a/v}$) are also computed which are not dependent on prevalence. These metrics are illustrated in Table 3, based on the terms defined in Table 2.

Table 3: Performance metrics for vessel classification.

Measure	Description
$SN_{a/v}$	$TP_{a/v}/(TP_{a/v}+FN_{a/v})$
$SP_{a/v}$	$TN_{a/v}/(TN_{a/v}+FP_{a/v})$
$ACC_{a/v}$	$(TP_{a/v}+TN_{a/v})/(TP_{a/v}+FP_{a/v}+TN_{a/v}+FN_{a/v})$
$CER_{a/v}$	$(FP_{a/v}+FN_{a/v})/(TP_{a/v}+FP_{a/v}+TN_{a/v}+FN_{a/v})$
$PPV_{a/v}$	$TP_{a/v}/(TP_{a/v}+FP_{a/v})$
$NPV_{a/v}$	$TN_{a/v}/(TN_{a/v}+FN_{a/v})$
$PLR_{a/v}$	$SN_{a/v}/(1-SP_{a/v})$
$NLR_{a/v}$	$(1-SN_{a/v})/SP_{a/v}$

3.2 Experimental Results

We have analysed the methodology by using 3149 vessel segments from 40 colour fundus images from 20 EPIC Norfolk participants. The algorithm is evaluated by using a two-fold validation methodology. The images of the right eye are assigned to set S_1 and the left eye images are allocated to the set S_2 . The classifier is then trained on S_1 and tested on S_2 , followed by training on S_2 and testing on S_1 . The performance metrics are computed separately for arterioles and venules and presented in Table 4.

Table 4: Vessel classification performance metrics.

Measure	Arterioles		Venules	
	Tested on S1	Tested on S2	Tested on S1	Tested on S2
$SN_{a/v}$	0.9067	0.8795	0.7658	0.7652
$SP_{a/v}$	0.7658	0.7836	0.9067	0.8804
$ACC_{a/v}$	0.8387	0.8298	0.8327	0.8261
$CER_{a/v}$	0.1612	0.1701	0.1672	0.1738
$PPV_{a/v}$	0.8162	0.8170	0.8757	0.8513
$NPV_{a/v}$	0.8757	0.8513	0.8162	0.8170
$PLR_{a/v}$	3.6183	5.7391	7.9255	8.8678
$NLR_{a/v}$	0.1261	0.1623	0.2763	0.2505

The similarity in the performance metrics obtained for the sets S_1 and S_2 indicates the repeatability of the methodology in classification of vessels. The sensitivity in the set S_1 for the arteries is 0.9067 and for the veins is 0.7658. This in turn indicates that the probability of incorrect classification (i.e., false positives) for arterioles and venules is 9.33% and 23.42% respectively. Some

results of the presented A/V classification methodology are illustrated in Figure 5.

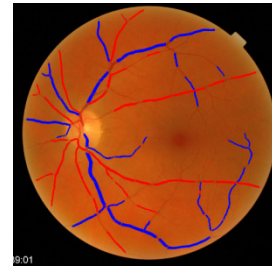


Figure 5: A/V classification result.

A comparison of the proposed method's performance metrics with the recently published methods is shown in Table 5. The sensitivity of proposed method in identifying arterioles is higher than the other methods, which suggests that our method has lower probability of incorrect classification. The higher specificity of our algorithm in identifying veins also indicates fewer false positives compared with other methods. We have analysed 40 coloured fundus images compared to 35, 58 and 35 images analysed in (Grisan and Ruggeri 2003), (Saez, González-Vázquez et al. 2012) and (Relan, MacGillivray et al. 2013), respectively. Also the resolution of our images are 3000 x 2000 pixels which is greater than 1300x1000 and 786x567 used in previous studies (Grisan and Ruggeri 2003) (Saez, González-Vázquez et al. 2012). It should be noted that the resolution of our test images is higher than those used to test other methods, so the performance metrics for our method may differ with a different image-set. The classification accuracy of the method is dependent upon the vessel segmentation results and the extraction of vessel centreline pixels. Moreover, the choice of a different classifier, feature set and retinal image zone is likely to have an impact of the method's performance.

Table 5: Results of our method compared with recently published methods.

	Method	SN	SP	PPV	NPV
Arteries	(Saez, González-Vázquez et al. 2012)	0.78	0.89	0.88	0.80
	(Relan, MacGillivray et al. 2013)	0.81	0.89	0.90	0.80
	Proposed Method	0.90	0.76	0.81	0.87
Veins	(Saez, González-Vázquez et al. 2012)	0.87	0.79	0.81	0.86
	(Relan, MacGillivray et al. 2013)	0.76	0.95	0.94	0.83
	Proposed Method	0.76	0.90	0.87	0.81

4 CONCLUSIONS

An automated method for A/V classification in retinal vasculature based on colour features utilizing the ensemble classifier of boot strapped decision trees is presented. To the best of our knowledge, this is the first time the decision trees based ensemble classifier has been used for A/V classification.

An application of image processing algorithms for computer assisted analysis of digital fundus images offers a number of advantages over a manual system, including fast, timely and reliable quantification of abnormalities. The presented methodology will be incorporated in to a software package QUARTZ (QUAntitative Analysis of Retinal vessel Topology and siZe). The QUARTZ software will assist in examining arterio-venous morphological associations with cardiovascular risk factors and outcomes in large population based studies, furthering our understanding of the vascular changes / consequences associated with the development of disease.

In future we aim to extend the QUARTZ software to incorporate the analysis of other retinal vessel features pathognomonic of cardiovascular disease, including measurement of arterio-venous ratio, identification of venous beading and quantification of arterio-venous nicking.

ACKNOWLEDGEMENTS

The authors would like to thank Professor Paul Foster and the European Investigation into Cancer in Norfolk (EPIC Norfolk) study for providing the retinal images used in this analysis. The EPIC Norfolk study is supported by grants from the Medical Research Council, Cancer Research UK and Research into Ageing.

REFERENCES

- Abràmoff, M. D., M. K. Garvin, et al. (2010). "Retinal Imaging and Image Analysis." *Biomedical Engineering, IEEE Reviews in 3*: 169-208.
- Dashtbozorg, B., A. M. Mendonca, et al. (2013). "An Automatic Graph-based Approach for Artery/Vein Classification in Retinal Images." *Image Processing, IEEE Transactions on PP(99)*: 1-1.
- EPIC-Norfolk. (2013). "European Prospective Investigation of Cancer (EPIC)." Retrieved September, 2013, from <http://www.srl.cam.ac.uk/epic/>.
- Fraz, M. M., S. A. Barman, et al. (2012). "An approach to localize the retinal blood vessels using bit planes and centerline detection." *Computer methods and programs in biomedicine 108(2)*: 600-616.
- Fraz, M. M., P. Remagnino, et al. (2013). "Quantification of blood vessel calibre in retinal images of multi-ethnic school children using a model based approach." *Computerized Medical Imaging and Graphics 37(1)*: 60-72.
- Fraz, M. M., P. Remagnino, et al. (2012). "Blood vessel segmentation methodologies in retinal images – A survey." *Computer methods and programs in biomedicine 108(1)*: 407-433.
- Fraz, M. M., P. Remagnino, et al. (2012). "An Ensemble Classification-Based Approach Applied to Retinal Blood Vessel Segmentation." *Biomedical Engineering, IEEE Transactions on 59(9)*: 2538-2548.
- Grisan, E. and A. Ruggeri (2003). A divide et impera strategy for automatic classification of retinal vessels into arteries and veins. *Engineering in Medicine and Biology Society, 2003. Proceedings of the 25th Annual International Conference of the IEEE*.
- Huang, Y., J. Zhang, et al. (2012). "An automated computational framework for retinal vascular network labeling and branching order analysis." *Microvascular Research 84(2)*: 169-177.
- Jack J. Kanski and Brad Bowling (2011). *Clinical Ophthalmology: A Systematic Approach*. London, Elsevier Health Sciences (UK).
- Nguyen, U., A. Bhuiyan, et al. (2013). "An Automated Method for Retinal Arteriovenous Nicking Quantification from Colour Fundus Images." *Biomedical Engineering, IEEE Transactions on PP(99)*: 1-1.
- Nguyen, U. T. V., A. Bhuiyan, et al. (2012). "An effective retinal blood vessel segmentation method using multi-scale line detection." *Pattern Recognition(0)*.
- Niemeijer, M., X. Xiayu, et al. (2011). "Automated Measurement of the Arteriolar-to-Venular Width Ratio in Digital Color Fundus Photographs." *Medical Imaging, IEEE Transactions on 30(11)*: 1941-1950.
- Owen, C. G., A. R. Rudnicka, et al. (2011). "Retinal Arteriolar Tortuosity and Cardiovascular Risk Factors in a Multi-Ethnic Population Study of 10-Year-Old Children; the Child Heart and Health Study in England (CHASE)." *Arteriosclerosis, Thrombosis, and Vascular Biology 31(8)*: 1933-1938.
- Polikar, R. (2006). "Ensemble Based Systems in Decision Making." *IEEE Circuits and Systems Magazine 6(3)*: 21-45.
- Relan, D., T. MacGillivray, et al. (2013). Retinal vessel classification: sorting arteries and veins. *35th Annual International Conference of the IEEE EMBS Engineering in Medicine and Biology Society (EMBC), Osaka, Japan, IEEE*.
- Ricci, E. and R. Perfetti (2007). "Retinal Blood Vessel Segmentation Using Line Operators and Support Vector Classification." *Medical Imaging, IEEE Transactions on 26(10)*: 1357-1365.
- Rothaus, K., X. Jiang, et al. (2009). "Separation of the retinal vascular graph in arteries and veins based upon

structural knowledge." *Image and Vision Computing* 27(7): 864-875.

Saez, M., S. González-Vázquez, et al. (2012). "Development of an automated system to classify retinal vessels into arteries and veins." *Computer methods and programs in biomedicine* 108(1): 367-376.

Vázquez, S. G., B. Cancela, et al. (2013). "Improving retinal artery and vein classification by means of a minimal path approach." *Machine Vision and Applications* 24(5): 919-930.

Wong, T. Y., R. Klein, et al. (2001). "Retinal microvascular abnormalities and incident stroke: the Atherosclerosis Risk in Communities Study." *The Lancet* 358(9288): 1134-1140.

The logo for SCITEPRESS features the word "SCITEPRESS" in a large, bold, sans-serif font. Below it, the words "SCIENCE AND TECHNOLOGY PUBLICATIONS" are written in a smaller, all-caps, sans-serif font. The text is overlaid on a faint, stylized background graphic that resembles a network or a map of connections.